Role of the Tropics and its Extratropical Teleconnections in State-Dependent Improvements of U.S. West Coast UFS Precipitation Forecasts

Wei-Ting Hsiao[1], Elizabeth A. Barnes[1], Eric D. Maloney[1], Stefan N. Tulich[2,3], Juliana Dias[3], and George N. Kiladis[3]

[1]Department of Atmospheric Science, Colorado State University, Fort Collins, Colorado, USA
[2]CIRES, University of Colorado Boulder, Boulder, Colorado, USA
[3]Physical Sciences Laboratory, NOAA, Boulder, Colorado, USA

Key Points:

- Nudging tropical fields in the UFS toward the observed state improves wintertime Weeks 3-4 precipitation forecasts over the U.S. West Coast
- A subset of initial states identified by multivariate k-means clustering exhibits greater precipitation forecast improvements with nudging
- Improved simulation of tropical intraseasonal variability when a strong Aleutian Low is present leads to these greater forecast improvements

Corresponding author: Wei-Ting Hsiao, `WeiTing.Hsiao@colostate.edu`

Abstract

Boreal-wintertime hindcasts in the Unified Forecast System with the tropics nudged toward reanalysis improve United States (U.S.) West Coast precipitation forecasts at Weeks 3-4 lead times when compared to those without nudging. To diagnose the origin of these improvements, a multivariate k-means clustering method is used to group hindcasts into subsets by their initial conditions. One cluster characterized by an initially strong Aleutian Low demonstrates larger improvements at Weeks 3-4 with nudging compared to others. The greater improvements with nudging for this cluster are related to the model error in simulating the interaction between the Aleutian Low and the teleconnection patterns associated with the Madden-Julian oscillation (MJO) and El Niño-Southern Oscillation (ENSO). Improving forecasts of tropical intraseasonal precipitation, especially during early MJO phases under non-cold ENSO, may be important for producing better Weeks 3-4 precipitation forecasts for the U.S. West Coast.

Plain Language Summary

To test whether a more accurate representation of tropical weather can lead to better extratropical forecasts Weeks 3-4 in advance during boreal winter, retrospective forecasts (hindcasts) are performed with the tropics forced to closely match observational estimates. The precipitation at Weeks 3-4 lead times is improved over the United States (U.S.) West Coast in an operational weather model in forced hindcasts compared to those without forcing. To diagnose the origin of these improvements, a machine-learning method that subsets hindcasts by the similarity of their initial weather states is used. One subset that demonstrates larger improvements at Weeks 3-4 than others features an initially strong low pressure system in the North Pacific. The greater improvements for this subset of hindcasts originate from an incorrect simulation of tropical precipitation in the non-forced hindcasts. In particular, the forced hindcasts are better able to simulate the weakening of the North Pacific low pressure a few weeks into the prediction that is produced by atmospheric waves emanating poleward induced by tropical precipitation. These findings identify under what conditions correctly simulating tropical precipitation is the most beneficial for Weeks 3-4 precipitation forecasts over the U.S. West Coast during boreal winter.

1 Introduction

Subseasonal-to-seasonal (S2S) predictability in the extratropics has been shown to partially originate in the tropics (Robertson et al., 2015). One source of predictability is provided by tropical-extratropical teleconnections that emerge approximately one week after being excited by a Rossby wave source in the subtropics, which is ultimately generated by upper-tropospheric tropical divergence associated with deep convection (Hoskins & Ambrizzi, 1993; Branstator, 2014). This mechanism has been established theoretically using linear Rossby wave theory (Hoskins & Karoly, 1981; Sardeshmukh & Hoskins, 1988), and its implications for S2S predictability have been investigated largely using conditional analysis from observations (e.g. Hendon et al., 2000; Matthews et al., 2004) and from weather model output (e.g. Ferranti et al., 1990; Vitart & Molteni, 2010). Exploring tropical sources of S2S predictability in operational weather forecast models may not only further provide insights into the mechanisms underlying this predictability, but may also provide model developers and forecast agencies information on when forecasts are more or less reliable, and which parts of the model to improve to elicit further forecast gains.

To investigate the tropical origins of global extended-range forecast skill during boreal winter and associated errors that can degrade forecast skill in an operational forecast system, a set of hindcasts were performed by Dias et al. (2021). Hindcasts over a twenty-year period were run with the tropics nudged toward reanalysis in an operational weather forecast model from the Unified Forecast System (UFS) developed by the National Oceanic and Atmospheric Administration (NOAA). Their results showed that with corrected representations of *tropical* horizontal winds, mass, temperature, and humidity fields, forecasts of precipitation and 500 hPa geopotential height (z500) are significantly improved in the Northern Hemisphere extratropics at Weeks 2-4 lead times. Notably, they also showed that forecast improvements due to tropical nudging are dependent on the initial state. For example, hindcasts are improved relatively more at four-week leads in the Northern Hemisphere extratropics with nudging when the Madden-Julian oscillation (MJO; Madden & Julian, 1971, 1972) is active at initialization.

Since tropical heating patterns, such as those associated with the MJO, are capable of exciting detectable and consistent teleconnection patterns in the extratropics (e.g. Ferranti et al., 1990; Matthews et al., 2004; Tseng et al., 2019), it is likely that extratropical forecasts in certain regions will be improved by correcting errors in predicted tropical heating, as suggested in previous studies (Ferranti et al., 1990; Bielli et al., 2010; Jung et al., 2010). Here, we investigate the specific initial states that lead to extratropical forecast improvements in the tropical nudging experiments described by Dias et al. (2021). Specifically, we condition forecast improvements of United States (U.S.) West Coast precipitation by their initial states using a multivariate clustering procedure, which will be shown to elucidate the underlying physical mechanisms more clearly as compared to conditioning on conventional climate indices. This approach allows us to investigate the specific initial states that yield the largest gains in forecast skill due to tropical nudging, without *a priori* assumptions of the exact physical phenomena associated with such improvements. We demonstrate that one cluster of hindcasts with a particular initial state shows greater forecast improvements than the others, and we scrutinize the mechanisms associated with these improvements due to tropical nudging.

2 Methodology

2.1 Model and Experimental Setup

Here, we utilize global hindcasts conducted by Dias et al. (2021) using a leading U.S. forecast model, specifically, version 15.1.1 of the NOAA/ National Centers for Environmental Prediction Global Forecast System (NOAA/NCEP GFS v15.1.1). Two types of hindcasts are verified against a model-generated reanalysis as described below. For details about the model configuration and initialization procedure, see Text S1 and Dias et al. (2021).

The verification dataset, ***ERAI-R***, is first produced by the model as a good approximation of the observed state represented by ERA-Interim reanalysis (Dee et al., 2011). The incremental analysis update (IAU; Bloom et al., 1996) scheme is utilized to nudge zonal and meridional winds, mass, temperature, and specific humidity over the whole globe in the model toward ERA-Interim during November 1999 to April 2018 for the extended boreal winter (November to April).

A set of hindcasts, ***FREE***, is performed to evaluate the forecast performance of the model in free-running mode (i.e. without nudging). In this setting, the model is run freely out to 30 days in each hindcast, where hindcasts are initialized every five days from the states in ERAI-R.

Another set of hindcasts, ***NUDGE***, is performed to assess the effect on S2S forecast performance in the extratropics when the tropics are represented accurately. The design of NUDGE is the same as FREE, except that the nudging method used in ERAI-R is applied within 30°S-30°N using a weighting function that is unity between 10°S-10°N, and is reduced to zero toward 30°S and 30°N (the same form of nudging is used in Jung et al., 2010). Although only dynamical and thermodynamical fields are nudged, this also results in significantly reduced tropical precipitation errors within the nudging region (see Fig. 5 in Dias et al., 2021).

2.2 Quantifying Forecast Performance of U.S. West Coast Precipitation

The present study puts emphasis on the forecast performance of precipitation along the U.S. West Coast and adjacent seas, which is assessed by its grid-wise area-averaged mean absolute error (MAE) over the region 30°N-50°N, 120°W-140°W (referred to as the U.S. West Coast; the box in the Figure 1 map) in FREE or NUDGE compared to ERAI-R. The improvements produced by NUDGE are quantified by the difference between the MAE of FREE and NUDGE. The precise bounds of U.S. West Coast spatial averaging domain do not affect our conclusions (not shown).

A multivariate k-means clustering analysis is performed to subset the hindcasts by their initial states. After assigning the number of desired clusters, k-means clustering partitions the data in a feature space by minimizing the within-cluster variance (Lloyd, 1982). This k-means clustering approach allows us to investigate the initial states associated with better forecast improvements due to tropical nudging, without *a priori* assumptions of the exact physical phenomena associated with the improvements. The data are processed in the following way before being input into the cluster analysis: (1) anomalies are calculated by subtracting daily climatologies from the fields of interest, where lead-dependent climatologies are used for the hindcasts; (2) empirical orthogonal functions (EOFs; Lorenz, 1956) of 20°S-90°N and 60°E-90°W precipitation and 200 hPa zonal wind (u200) anomalies are computed based on the uncentered covariance matrices of each variable; (3) the dimensionless principal components (PCs) of all of the EOFs are weighted by their variance explained; (4) the weighted PCs from the two variables are stacked to form a feature vector which is used as input to the k-means clustering algorithm. The choice of using precipitation and u200 to characterize the initial state is motivated by their importance for representing the tropical forcing pattern and the tropical-to-extratropical Rossby wave guide (Trenberth et al., 1998), respectively. We implement the k-means clustering algorithm by *scikit-learn* v0.23.2 (Pedregosa et al., 2011) with the default settings except for $K = 8$ (i.e. 8 clusters) and setting the initialization seed to 0. Similar conclusions hold for $K = 8$ to 15 and with four random initialization seeds (0, 1, 2, and 3 as integers) for each K (not shown), however. Values of K below 8 seldom identify clusters with robust improvements in forecast performance.

To associate the clusters with known modes of climate variability, we also use metrics that represent the states of the MJO and El Niño-Southern Oscillation (ENSO). The outgoing longwave radiation MJO index (OMI; Kiladis et al., 2014) is used to assess the intensity of the MJO and its phases, where an MJO event is defined as any period when the magnitude of OMI ≥ 1. The multivariate ENSO Index Version 2 (MEIv2; Zhang et al., 2019) is used to quantify ENSO states. A dichotomy of ENSO states is used in this study, and we use the terminology non-warm ENSO to represent MEIv2 < 0, and non-cold ENSO for MEIv2 ≥ 0.

3 Results

Nudging in the tropics generally improves the Weeks 3-4 (Days 15-28) precipitation forecast performance over the U.S. West Coast with the distribution of the MAE shifted toward smaller values in NUDGE compared to FREE (Figure 1). The peak of the MAE distribution is reduced by about 1 mm day^{-1} in NUDGE, while the average and the median are reduced by 0.67 and 0.68 mm day^{-1}, respectively. Improvements in NUDGE relative to FREE emerge primarily during Week 3, as shown by the right tails of the weekly distribution of MAE reduction (Figure S1), suggesting that processes on S2S timescales are responsible for the improvements. Overall, nudging improves the forecast performance over the U.S. West Coast, particularly for those cases in FREE that are relatively poor in the Weeks 3-4 range (Figure S2), as also discussed by Dias et al. (2021).

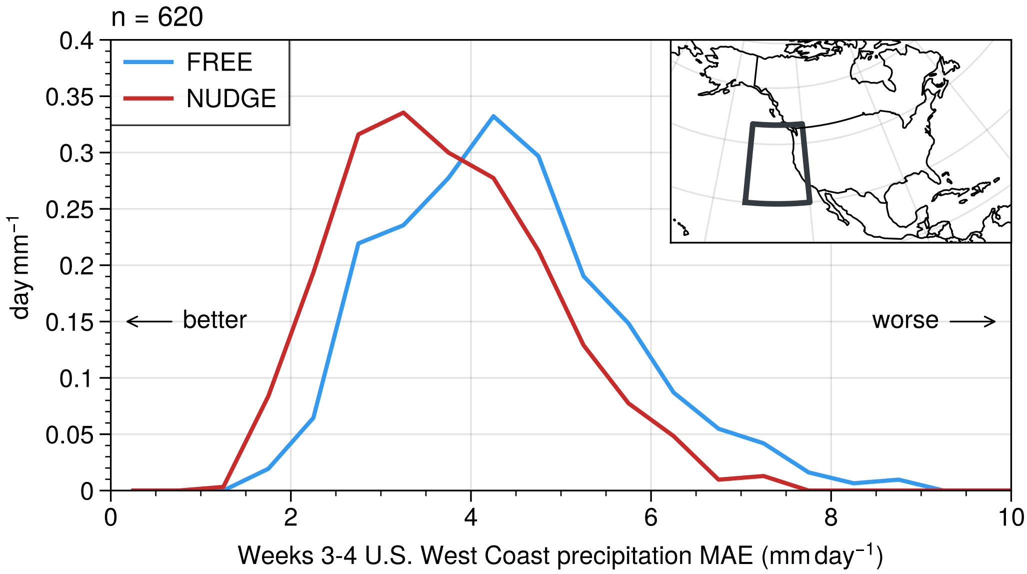

Figure 1. The distribution of U.S. West Coast precipitation MAE averaged over Weeks 3-4 from FREE (blue line) and from NUDGE (red line). MAE is averaged over the area shown in the map (see main text).

Next, we subdivide the forecast improvements by cluster to investigate whether there are state-dependent improvements with nudging (see Figure S3 for the composite initial states of all the clusters). Cluster #4 exhibits distinctly larger improvements compared to the other seven clusters (Figure 2b), and has a significantly larger number of hindcasts with large MAE reductions compared to reductions composited over all clusters (Figure 2a). The initial states of Cluster #4 are associated with non-cold ENSO conditions and are primarily associated with MJO phases 8, 1, and 2, with the presence of an enhanced Aleutian Low (Figure 3a) and anomalous positive U.S. West Coast precipitation anomalies (Figure S3).

To understand why Cluster #4 tends to be associated with distinctly larger improvements under nudging, it is helpful to explore how the forecast composites evolve differently in NUDGE versus FREE, as compared to ERAI-R. Over the first two weeks of the forecast, both FREE and NUDGE exhibit an enhanced Aleutian Low in the North Pacific and enhanced U.S. West Coast precipitation, in accordance with ERAI-R (top two rows of Figure 3b-d). Over Weeks 1-2, the primary state of the MJO progresses from phases 8 to 2 (as shown by the top two rows of Figure 3d). During Week 3, the anomalous Aleutian Low and U.S. West Coast precipitation are weakened in NUDGE, broadly mirroring what is seen in ERAI-R (third row of Figure 3c-d). However, this weakening trend is less pronounced in FREE, which instead shows strengthening of precipitation along the coast of California (third row of Figure 3b). During Week 4, anomalously low z500 is present over the North Pacific and the southern U.S., but with different spatial patterns in each set of simulations. Furthermore, U.S. West Coast precipitation anomalies are also quite different across the three simulations in Week 4 (bottom row of Figure 3b-d), with FREE exhibiting a strong positive precipitation anomaly in the southwest U.S. that is not present in the other two runs.

We hypothesize that the correction of intraseasonal tropical precipitation and its associated teleconnection pattern under the presence of non-cold ENSO-like states is the source of the robust forecast improvements in Week 3 for Cluster #4. ERAI-R indicates

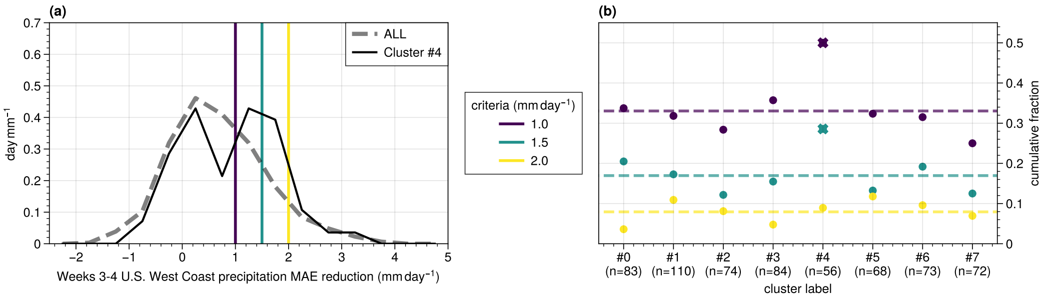

Figure 2. (a) The distribution of Weeks 3-4 U.S. West Coast precipitation MAE reduction associated with tropical nudging from all cases (ALL; bold gray line) and from Cluster #4 (solid black line). (b) The fraction of hindcasts having an MAE reduction greater than the thresholds as defined by the vertical lines in (a) for the ALL curve (horizontal dashed lines) and from the curve for each of the clusters (symbols). For clarity, only the distribution for Cluster #4 is shown in (a) as the solid black curve. The symbols marked as crosses are significantly different ($p <$ 0.05) from the baseline fractions (horizontal dashed lines) using a two-tailed bootstrapping test with 10000 realizations.

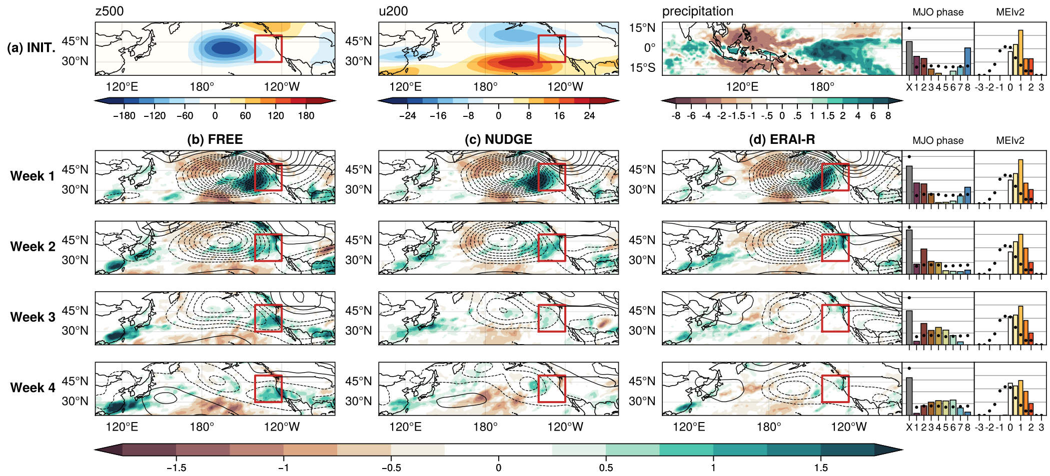

Figure 3. (a) the row shows the composited Day-1 states in ERAI-R: z500 (left; m), u200 (middle; m s^{-1}), and precipitation (right; mm day^{-1}) anomalies from Cluster #4. The lower rows are the composites of weekly precipitation (shading; mm day^{-1}) and z500 (contours; 10-m spacing with zero omitted) anomalies for Cluster #4 in (b) FREE, (c) NUDGE, and (d) ERAI-R as columns. The red box indicates where U.S. West Coast precipitation errors are assessed. The bar charts attached to the right column show the fraction of dates within Cluster #4 that fall in each MJO phase (non-MJO days are indicated by X) and ENSO index (MEIv2; with interval 0.5 centered at 0) for each range of lead times, where the black dots indicate the underlying fractions for all the extended boreal wintertime dates, and the gray horizontal reference lines are spaced by 10% starting at 0 at the bottom.

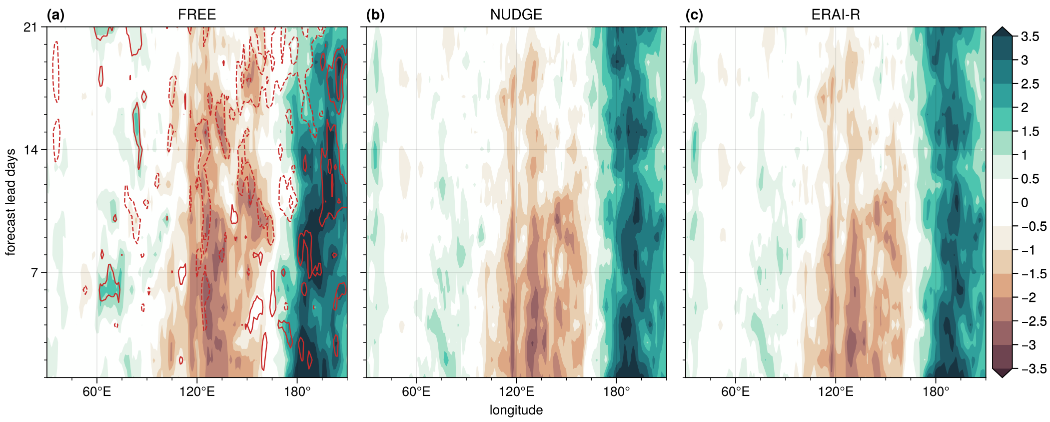

Figure 4. Hovmöller plots of the daily composite anomalies of 10°S-10°N precipitation (shading; mm day^{-1}) for Cluster #4 in (a) FREE, (b) NUDGE, and (c) ERAI-R. The contours in (a) and (b) show the precipitation anomaly differences between the hindcasts and ERAI-R with 1 mm day^{-1} spacing. The zero line is omitted.

that the initial states selected by Cluster #4 are associated with an enhanced Aleutian Low. This is similar to that associated with El Niño events and is also consistent with the constructive interference between non-cold ENSO and the time-lagged response to MJO phases 6-7 (Henderson & Maloney, 2018). Over Weeks 1-2, similar anomalies as shown at the initial state persist with enhanced U.S. West Coast precipitation (top two rows in Figure 3d). In Week 2, a higher frequency of MJO phase 2 events is present (second row in Figure 3d), which is expected to excite a negative Pacific-North America (PNA) teleconnection pattern associated with positive geopotential anomalies in the Aleutian Low region in Week 3 (Tseng et al., 2019). Combined with a non-cold ENSO state that is associated with a positive PNA pattern and anomalous Aleutian Low, destructive interference occurs that weakens the Low as shown in Henderson and Maloney (2018). This further decreases U.S. West Coast precipitation by reducing moisture transport associated with the anomalous Aleutian Low (Xiong et al., 2019), a process that is well represented in ERAI-R and also in the NUDGE hindcasts (third row in Figure 3c-d). This dynamical response is much less robust in FREE (third row in Figure 3b), which we hypothesize is caused by an incorrect simulation of upper-level divergence associated with precipitation in the tropics and their teleconnections. Figure 4a shows that large precipitation errors exist in the deep tropics (contours) in FREE after Day 7. In particular, the model produces precipitation anomalies of excessive magnitude that resemble those anomalies associated with non-cold ENSO events, and fails to simulate the reduction after Day 7 when MJO precipitation begins to move across the Maritime Continent (shown in Figure 3d with the most frequent MJO phases transitioning from phases 8-2 in Week 1 to phases 2-4 in Week 2). Since precipitation anomalies in the deep tropics are associated with upper troposphere divergent wind anomalies that can generate stationary Rossby waves in the presence of a background vorticity gradient (Sardeshmukh & Hoskins, 1988), it is likely that this precipitation error in FREE leads to failure in simulating the correct Rossby wave pattern over the North Pacific. Subsequently, it leads to incorrect simulation of the Aleutian Low and results in U.S. West Coast precipitation errors that are improved with nudging.

Although the mechanism described above appears to explain Week 3, during Week 4, North Pacific z500 and precipitation anomalies in ERAI-R start to become diverse within Cluster #4 as demonstrated by an increasingly large spread in the MJO phase distribution in Figure 3d. Furthermore, phases 4-6 of the MJO become more common in Week

3, which were shown by Tseng et al. (2019) to produce inconsistent teleconnections to the North Pacific. Hence, a strongly forced signal with consistent sign from the extratropics is less likely to be reflected in the composite mean, and the consistency between the composites likely no longer serves as an indicator of forecast performance. Instead, a hindcast-by-hindcast comparison is needed to evaluate the performance. Spatial correlation coefficients of Week-4 z500 anomalies over the North Pacific (20°N-70°N, 150°E-120°W) between FREE and ERAI-R and between NUDGE and ERAI-R are calculated to assess the midlatitude z500 forecast improvements due to tropical nudging (Figure S4). The average correlation coefficient among hindcasts is +0.17 between FREE and ERAI-R and +0.41 between NUDGE and ERAI-R, meaning that nudging improves the overall spatial representation of midlatitude z500 over Week 4, even though there may not be a consistently-signed signal from the tropics that forces the composite mean. However, when subsetting the hindcasts to isolate only those with the largest forecast improvements in Cluster #4, the enhanced Aleutian Low as well as the increased U.S. West Coast precipitation anomalies are shown to robustly persist over Week 4 in a composite analysis in FREE but not in NUDGE and ERAI-R (Figure S5). This suggests that the hypothesis of destructive interference may still be applicable to those cases in Week 4 where NUDGE performs particularly well relative to FREE.

These results strongly point to the importance of correctly representing the tropics for Weeks 3-4 extratropical precipitation forecasts. While we have proposed a physical mechanism to explain the enhanced improvements in Cluster #4 with tropical nudging, we still have not addressed why Cluster #4 alone provides larger forecast improvements relative to other clusters. We propose some possible reasons here. First, there is greater opportunity for forecast errors and improvements when the precipitation magnitudes in ERAI-R are already large. This is the case for Clusters #3, #4 and #5, as seen in Figure S3. Second, precipitation over the Indo-Pacific warm pool region (10°S-10°N, 60°E-170°E) has been shown to generate teleconnection patterns that strongly affect U.S. West Coast weather on S2S timescales (Tseng et al., 2019), with MJO phases 2 and 3 providing particularly strong forcing 7-10 days later. Compared to other phases, precipitation over the Indo-Pacific warm pool region is represented relatively poorly in the model during MJO phases 2-4 and therefore improves more with nudging (Figure S6). Only Cluster #2, #4, and #5 show a higher frequency of MJO phases 2-4 compared to the underlying MJO phase distribution at Weeks 1-2 leads (Figure S7), suggesting that error reductions in the associated dynamical response are likely also greater in those clusters. Third, the background states of different clusters provide different waveguide properties for stationary Rossby waves. Thus, it is possible that the U.S. West Coast is less modulated by teleconnections in other clusters than Cluster #4, while other geographical locations might show a stronger modulation.

The multivariate k-means clustering method is capable of capturing features in the initial states important for U.S. West Coast forecast improvements, which includes a strong anomalous Aleutian Low. Conditioning the hindcasts on ENSO index and MJO phase (e.g. MEIv2 ≥ 0 and MJO phases 1, 4, and 8; Figure S8), rather than using k-means clustering, also yields statistically significant forecast improvements. This is perhaps not surprising, as it is well known that ENSO and MJO teleconnections can also modulate the Aleutian Low (e.g. Henderson & Maloney, 2018). However, for example, the composites of all hindcasts with non-cold ENSO that are initially in MJO phases 8 and 1 do not show an enhanced Aleutian Low as strong as in Cluster #4 (Figure S9). This is possibly because not all MJO and ENSO events in these phases strongly modulate the Aleutian Low. For instance, the strength of the MJO teleconnection to the extratropics is also modulated by other factors such as the strength of the tropical quasi-biennial oscillation (QBO; Toms et al., 2020). The k-means clustering approach thus allows us to focus on initial states that feature an enhanced anomalous Aleutian Low, whether or not those days map onto specific climate indices (see the relatively wide spread of MJO phases and ENSO indices in the bar chart of Figure 3a). Here, we leverage the advantage of clustering and propose an underlying mechanism that would have been more difficult to isolate using MJO and ENSO metrics alone.

4 Summary

Extended-range precipitation forecast improvements over the U.S. West Coast in NOAA/NCEP GFS v15.1.1 are examined in hindcasts where tropical fields of horizontal winds, mass, temperature, and humidity are nudged toward observations. With nudging, the forecast mean absolute error of U.S. West Coast precipitation is reduced over Weeks 3-4 (Figure 1 and Figure S1), with larger reductions during forecast periods that were particularly poorly simulated in the FREE simulations where nudging is not applied (Figure S2). This is consistent with the findings in Dias et al. (2021).

A conditional forecast improvement analysis is performed based on a multivariate clustering method. One specific cluster (Cluster #4), characterized by initial states with a strong Aleutian Low and weighted toward non-cold ENSO conditions and MJO phases 8-2 (Figure 3a), is shown to provide significantly larger forecast improvements in U.S. West Coast precipitation (Figure 2). The robust improvements can be explained by an interaction that is not simulated well in the free-running simulations (FREE), but is well-represented in the nudged simulations (NUDGE): a strong Aleutian Low is subsequently weakened after two weeks by the destructive interference associated with the MJO phases 8-2 teleconnection pattern (Figure 3b-d) under non-cold ENSO conditions. The poor representation of tropical intraseasonal precipitation variability in the FREE simulations (Figure 4a) is suggested to produce an unrealistic interaction between the Aleutian Low and the MJO teleconnection pattern, leading to errors in the z500 and precipitation pattern near the U.S. West Coast. These errors are attenuated in the nudged simulations (Figure 3b-d and Figure 4b).

We did not perform an exhaustive evaluation of the model improvements for every cluster, choosing instead to concentrate on Cluster #4 since it exhibits substantially greater improvements for U.S. West Coast precipitation in Weeks 3-4. It is possible that other clusters provide better forecast improvements with nudging at other geographical locations, which could be examined in a future study. More sets of tropical nudging experiments, including those with nudging only being applied for a narrower latitudinal band, and over shorter time periods including over only the first week or two of the hindcasts, were also conducted by Dias et al. (2021). These experiments might also be useful for examining some of the proposed mechanisms above.

Note that the clustering method provides an alternative to using conventional ENSO and MJO metrics to analyze conditional forecast improvements. The clustering method shows that forecast improvements for U.S. West Coast precipitation is largest when an anomalously strong Aleutian Low is present in the initial condition, which subsequently gets perturbed by the evolution of the tropics. A major implication of this study is that improving forecasts of intraseasonal precipitation evolution in the tropics, especially that during MJO phases 8 and 1-4 under non-cold ENSO states, might be key to producing better U.S. West Coast precipitation forecasts.

Acknowledgments
This work was funded, in part, by NOAA grants NA19OAR4590151 and NA18OAR4310299, and NSF grant AGS-1841754.

Open Research

Model, algorithm packages, and data, including those being used as model boundary and initial conditions, can be accessed online (NOAA/NCEP GFS v15.1.1: `https://`

www.emc.ncep.noaa.gov/emc/pages/numerical_forecast_systems/gfs/implementations.php; GEFSv12: https://www.emc.ncep.noaa.gov/emc/pages/numerical_forecast_systems/gefs.php; scikit-learn v0.23.2: https://scikit-learn.org/0.23/; ERA-Interim: https://apps.ecmwf.int/datasets/data/interim-full-daily/; OMI: https://www.psl.noaa.gov/mjo/mjoindex/omi.1x.txt; MEIv2: https://psl.noaa.gov/enso/mei/data/meiv2.data). The output from ERAI-R, FREE, and NUDGE with large data size (about 70 terabytes) is stored on NOAA High Performance Storage and will be provided upon request, whereas readers can reproduce the output using the model setting described in Dias et al. (2021).

References

Bielli, S., Douville, H., & Pohl, B. (2010, July). Understanding the west african monsoon variability and its remote effects: an illustration of the grid point nudging methodology. *Clim. Dyn.*, *35*(1), 159–174.

Bloom, S. C., Takacs, L. L., da Silva, A. M., & Ledvina, D. (1996, June). Data assimilation using incremental analysis updates. *Mon. Weather Rev.*, *124*(6), 1256–1271.

Branstator, G. (2014, December). Long-Lived response of the midlatitude circulation and storm tracks to pulses of tropical heating. *J. Clim.*, *27*(23), 8809–8826.

Dee, D. P., Uppala, S. M., Simmons, A. J., Berrisford, P., Poli, P., Kobayashi, S., ... Vitart, F. (2011, April). The ERA-Interim reanalysis: configuration and performance of the data assimilation system. *Quart. J. Roy. Meteor. Soc.*, *137*(656), 553–597.

Dias, J., Tulich, S. N., Gehne, M., & Kiladis, G. N. (2021, June). Tropical origins of weeks 2-4 forecasts errors during northern hemisphere cool season. *Mon. Weather Rev.*, *-1*(aop).

Ferranti, L., Palmer, T. N., Molteni, F., & Klinker, E. (1990, September). Tropical-Extratropical interaction associated with the 30–60 day oscillation and its impact on medium and extended range prediction. *J. Atmos. Sci.*, *47*(18), 2177–2199.

Henderson, S. A., & Maloney, E. D. (2018, July). The impact of the Madden–Julian oscillation on High-Latitude winter blocking during el niño–southern oscillation events. *J. Clim.*, *31*(13), 5293–5318.

Hendon, H. H., Liebmann, B., Newman, M., Glick, J. D., & Schemm, J. E. (2000, January). Medium-Range forecast errors associated with active episodes of theMadden–Julian oscillation. *Mon. Weather Rev.*, *128*(1), 69–86.

Hoskins, B. J., & Ambrizzi, T. (1993, June). Rossby wave propagation on a realistic longitudinally varying flow. *J. Atmos. Sci.*, *50*(12), 1661–1671.

Hoskins, B. J., & Karoly, D. J. (1981, June). The steady linear response of a spherical atmosphere to thermal and orographic forcing. *J. Atmos. Sci.*, *38*(6), 1179–1196.

Jung, T., Miller, M. J., & Palmer, T. N. (2010, June). Diagnosing the origin of Extended-Range forecast errors. *Mon. Weather Rev.*, *138*(6), 2434–2446.

Kiladis, G. N., Dias, J., Straub, K. H., Wheeler, M. C., Tulich, S. N., Kikuchi, K., ... Ventrice, M. J. (2014). A comparison of OLR and Circulation-Based indices for tracking the MJO. *Mon. Weather Rev.*, *142*(5), 1697–1715.

Lloyd, S. P. (1982). Least squares quantization in pcm. In *IEEE transactions on information theory.*

Lorenz, E. N. (1956). Empirical orthogonal functions and statistical weather prediction.

Madden, R. A., & Julian, P. R. (1971, July). Detection of a 40–50 day oscillation in the zonal wind in the tropical pacific. *J. Atmos. Sci.*, *28*(5), 702–708.

Madden, R. A., & Julian, P. R. (1972). Description of global-scale circulation cells in the tropics with a 40–50 day period. *J. Atmos. Sci.*, *29*(6), 1109–1123.

Matthews, A. J., Hoskins, B. J., & Masutani, M. (2004, July). The global response to tropical heating in the Madden–Julian oscillation during the northern winter. *Quart. J. Roy. Meteor. Soc.*, *130*(601), 1991–2011.

Pedregosa, F., Varoquaux, G., Gramfort, A., Michel, V., Thirion, B., Grisel, O., ... Duchesnay, É. (2011). Scikit-learn: Machine learning in python. *J. Mach. Learn. Res.*, *12*(85), 2825–2830.

Robertson, A. W., Kumar, A., Peña, M., & Vitart, F. (2015, March). Improving and promoting subseasonal to seasonal prediction. *Bull. Am. Meteorol. Soc.*, *96*(3), ES49–ES53.

Sardeshmukh, P. D., & Hoskins, B. J. (1988, April). The generation of global rotational flow by steady idealized tropical divergence. *J. Atmos. Sci.*, *45*(7), 1228–1251.

Toms, B. A., Barnes, E. A., Maloney, E. D., & Heever, S. C. (2020, April). The global teleconnection signature of the madden-julian oscillation and its modulation by the quasi-biennial oscillation. *J. Geophys. Res.*, *125*(7).

Trenberth, K. E., Branstator, G. W., Karoly, D., Kumar, A., Lau, N.-C., & Ropelewski, C. (1998, June). Progress during TOGA in understanding and modeling global teleconnections associated with tropical sea surface temperatures. *J. Geophys. Res.*, *103*(C7), 14291–14324.

Tseng, K.-C., Maloney, E., & Barnes, E. (2019, January). The consistency of MJO teleconnection patterns: An explanation using linear rossby wave theory. *J. Clim.*, *32*(2), 531–548.

Vitart, F., & Molteni, F. (2010, April). Simulation of the madden- julian oscillation and its teleconnections in the ECMWF forecast system. *Quart. J. Roy. Meteor. Soc.*, *136*(649), 842–855.

Xiong, Y., Chen, Q., & Ren, X. (2019, January). Influence of boreal winter intraseasonal variation of aleutian low on water vapor transport and atmospheric rivers. *Atmosphere*, *10*(2), 49.

Zhang, T., Hoell, A., Perlwitz, J., Eischeid, J., Murray, D., Hoerling, M., & Hamill, T. M. (2019, September). Towards probabilistic multivariate ENSO monitoring. *Geophys. Res. Lett.*, *46*(17-18), 10532–10540.

Figure 1.pdf.

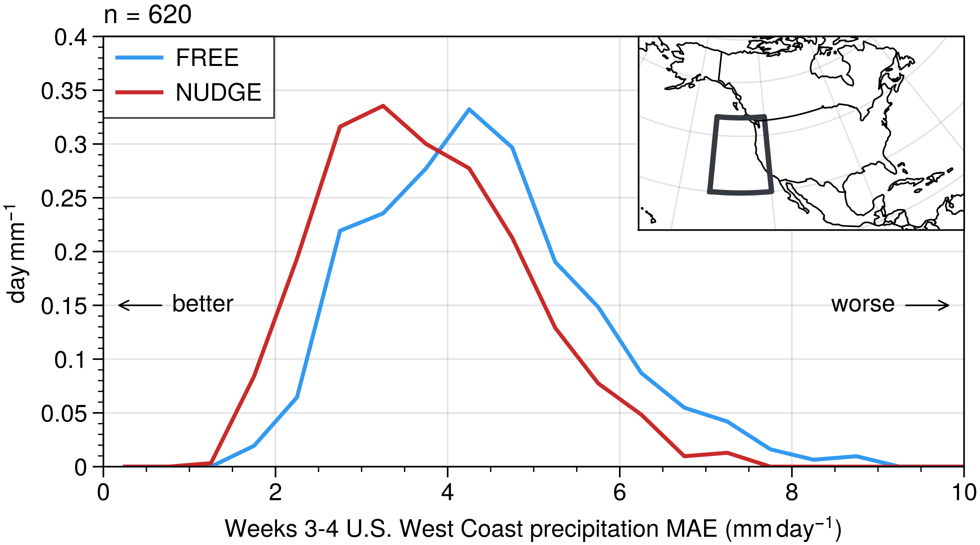

n = 620
FREE
NUDGE
day mm^{-1}
0.4
0.35
0.3
0.25
0.2
0.15
0.1
0.05
0
← better
worse →
0
2
4
6
8
10
Weeks 3-4 U.S. West Coast precipitation MAE (mm day^{-1})

Figure 2.pdf.

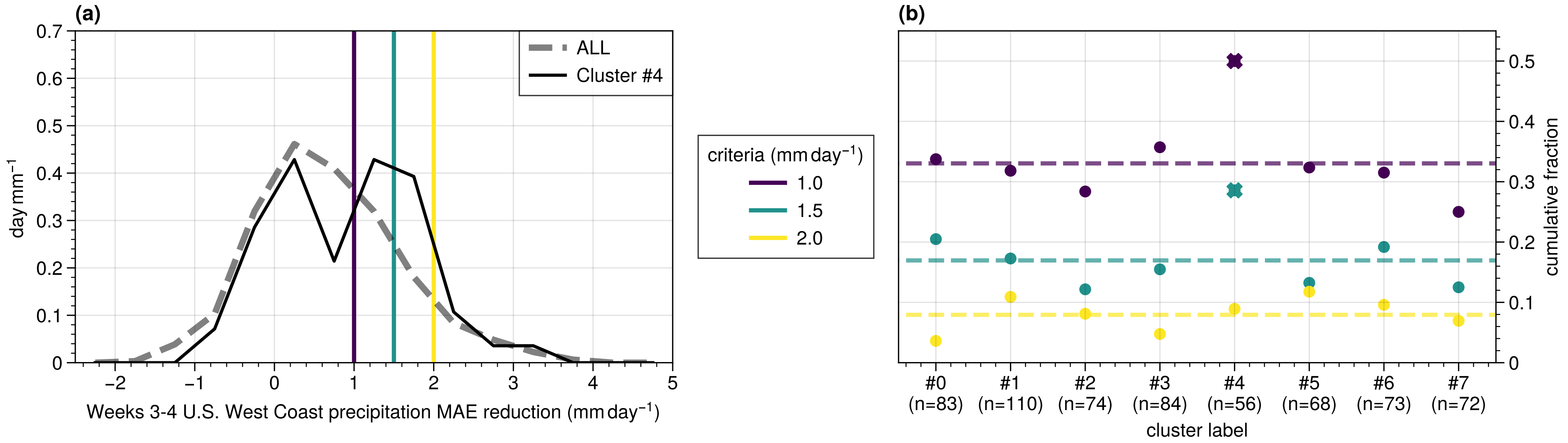

(a)
(b)
ALL
Cluster #4
criteria (mm day⁻¹)
1.0
1.5
2.0
day mm⁻¹
Weeks 3-4 U.S. West Coast precipitation MAE reduction (mm day⁻¹)
cumulative fraction
cluster label
#0 (n=83)
#1 (n=110)
#2 (n=74)
#3 (n=84)
#4 (n=56)
#5 (n=68)
#6 (n=73)
#7 (n=72)

Figure 3.pdf.

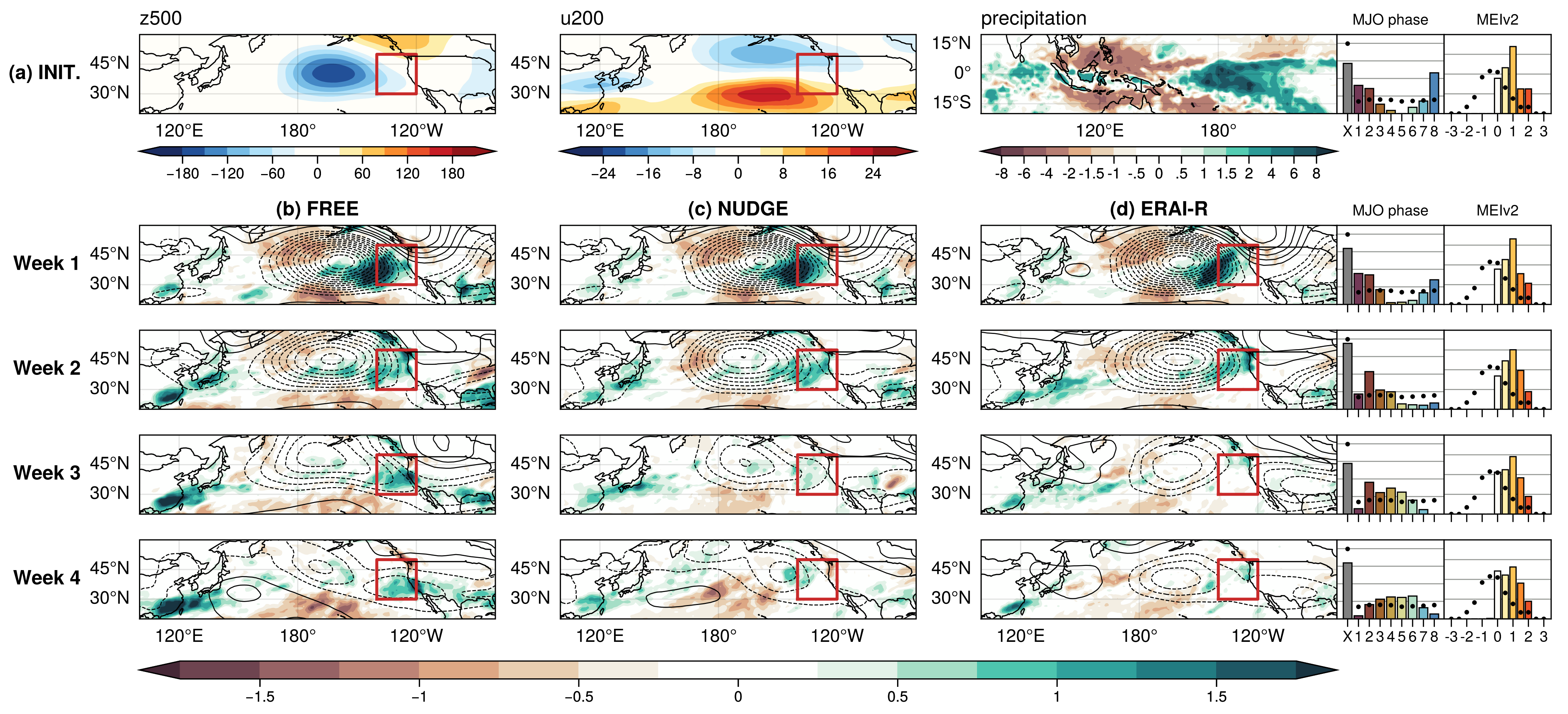

z500
u200
precipitation
MJO phase
MEIv2
(a) INIT.
45°N
30°N
15°N
0°
15°S
120°E
180°
120°W
X 1 2 3 4 5 6 7 8
-3 -2 -1 0 1 2 3
−180 −120 −60 0 60 120 180
−24 −16 −8 0 8 16 24
-8 -6 -4 -2 -1.5 -1 -.5 0 .5 1 1.5 2 4 6 8
(b) FREE
(c) NUDGE
(d) ERAI-R
Week 1
Week 2
Week 3
Week 4
−1.5 −1 −0.5 0 0.5 1 1.5

Figure 4.pdf.

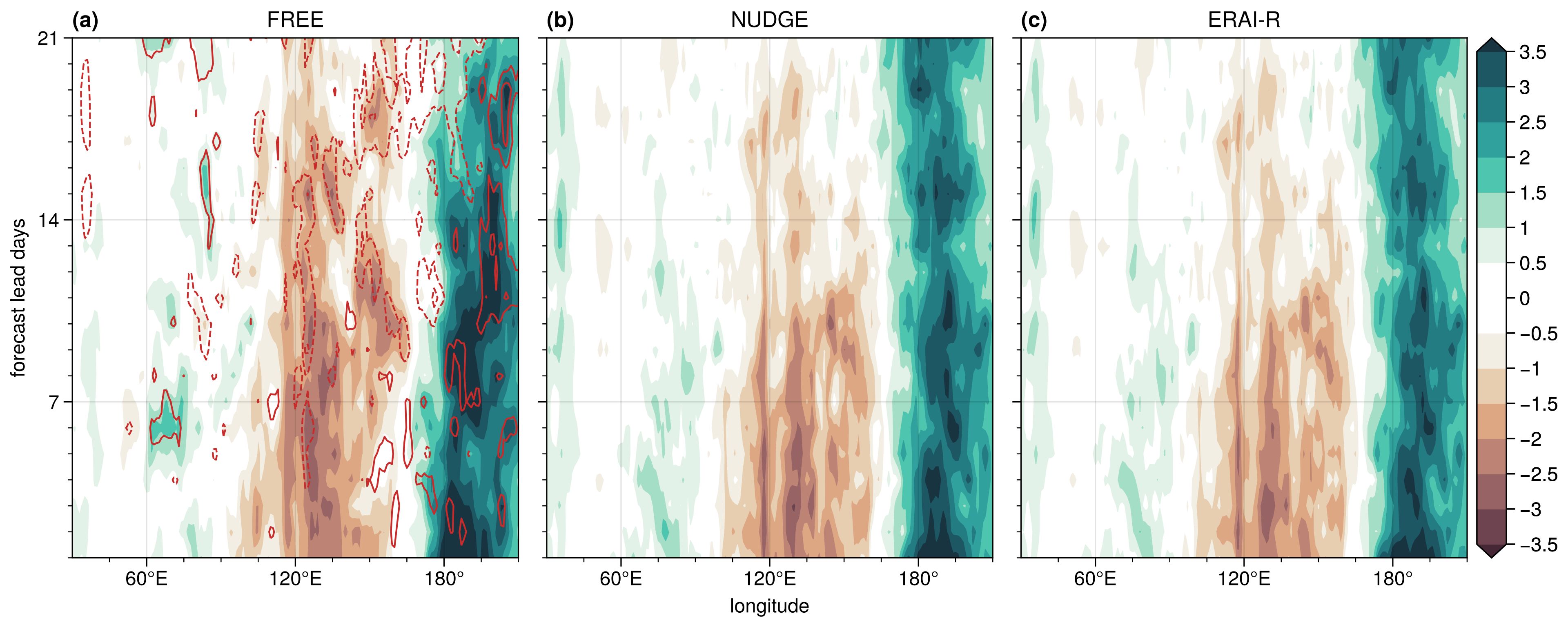

(a)
FREE
(b)
NUDGE
(c)
ERAI-R
21
14
7
forecast lead days
60°E
120°E
180°
longitude
3.5
3
2.5
2
1.5
1
0.5
0
−0.5
−1
−1.5
−2
−2.5
−3
−3.5